Biosensors and Bioelectronics 49 (2013) 450–456

Contents lists available at SciVerse ScienceDirect

Biosensors and Bioelectronics

journal homepage: www.elsevier.com/locate/bios

# Glycated hemoglobin ($HbA_{1c}$) affinity biosensors with ring-shaped interdigital electrodes on impedance measurement

Ku-Meng Hsieh [a], Kung-Chieh Lan [a], Wei-Li Hu [a], Ming-Kun Chen [a], Ling-Sheng Jang [a], Min-Haw Wang [b,*]

[a] Department of Electrical Engineering and Center for Micro/Nano Science and Technology, National Cheng Kung University, Taiwan
[b] Department of Electrical Engineering, Chinese Culture University, Da Yi Building 3F, 55 Huagang Road, Shilin Chiu, Taipei 111, Taiwan

ARTICLE INFO

*Article history:*
Received 4 February 2013
Received in revised form
30 May 2013
Accepted 31 May 2013
Available online 11 June 2013

*Keywords:*
Glycated hemoglobin ($HbA_{1c}$)
Ring-shaped interdigital electrodes (RSIDEs)
Self-assembled monolayer (SAM)
Thiophene-3-boronic acid (T3BA) Boronic Affinity
Impedance measurement
Capacitor biosensor

ABSTRACT

Glycated hemoglobin ($HbA_{1c}$) is one of the most important diagnostic assays for the long-term mark of glycaemic control in diabetes. This study presents an affinity biosensor for $HbA_{1c}$ detection which is label-free based on the impedance measurement, and it features low cost, low sample volume, and requires no additional reagent in experiments. The ring-shaped interdigital electrodes (RSIDEs) are designed to promote the distribution uniformity and immobilization efficiency of $HbA_{1c}$, and are further employed to characterize the impedance change and identify various concentrations of $HbA_{1c}$. The self-assembled monolayer (SAM) of thiophene-3-boronic acid (T3BA) is provided to modify the gold electrode surface. Afterwards, the esterification reaction between $HbA_{1c}$ and T3BA produces a relative change of electrical property on the electrode surface. The RSIDEs with SAM of T3BA exhibit a wide range from 100 to 10 ng/μL producing an approximate logarithmic decrease of impedance, a low detection limit of 1 ng/μL, a good selectivity and short-term stability for $HbA_{1c}$ determination. The remarkable advantages (miniaturization and low-cost) fill the bill of point-care diagnostics for portable sensor development.



## 1. Introduction

In the past decades, diabetes mellitus has become a serious global health problem, reaching the level of epidemic proportions in many developed countries (King and Rewers, 1993). According to the 2010 worldwide projection statistics, there are more than 220 million diabetics, with most suffering from Type 2 Diabetes (Amos et al., 1997). Therefore, research in diabetes mellitus, such as comprehension of pathogenesis and prevention or amelioration of their long-term complications, has become more and more important (Krishnamurti and Steffes, 2001).

$HbA_{1c}$ has turned into one of the most significant diagnostic assays for long-term glycaemic control since 1970s. $HbA_{1c}$ is generated by a non-enzymatic reaction between glucose and the amino-terminal valine of the hemoglobin's beta chain (Bunn et al., 1975). The ratio represents an average blood glucose level over the 100 to 120-day lifespan for red blood cells. Moreover, this ratio can improve the distortions of common blood glucose levels that might be affected by daily diet, exercise, medicine, and disease. For $HbA_{1c}$ detection, the most commonly recommended methods include cation-exchange chromatography (Tanakaa et al., 2009), electrophoresis (Jenkins and Ratnaike, 2005), mass spectrometry (Busto et al., 2008), and boronate-affinity chromatography (Li et al., 2001; Huang et al., 2011). However, most of these methodologies demand technical instruments and multiple operation steps, resulting in portability difficulties for meeting clinical demands. Consequently, electrical biosensors have received increasing amounts of attention over the past decades.

Numerous immunosensors and electrochemical biosensors for $HbA_{1c}$ detection have been reported recently, and although the required sample volume and overall device size have been reduced, detection remains time-consuming (Stöllner et al., 2002; Fanga et al., 2009). Additionally, such devices and the related tests are expensive due to the use of $HbA_{1c}$/hemoglobin antibodies to induce the specific labeling of $HbA_{1c}$/hemoglobin (Qu et al., 2009; Xue et al., 2011a, 2011b, 2010). By contrast, a fast, cheap and convenient device can be realized by boronic acid binding. In order to complete label-free detection of biosensors, boronic acid–diol interaction is an important application which separates $HbA_{1c}$ from non-$HbA_{1c}$ via boronic acid affinity (Son et al., 2010; Přibyl and Skládal, 2005, 2006; Halámeka et al., 2007).

The binding behavior of the electrode surface can still be detected at a specific frequency range, despite the absence of reagents (Lasseter et al., 2004). Furthermore, low sensitivity means that only high concentrations can be detected, which constitutes a

* Corresponding author. Tel.: +886 228610511#33205; fax: +886 228625230.
*E-mail addresses:* min_how@yahoo.com.tw, g893119@alumni.nthu.edu.tw (M.-H. Wang).

0956-5663/$ - see front matter © 2013 Elsevier B.V. All rights reserved.
http://dx.doi.org/10.1016/j.bios.2013.05.059

problem since an $HbA_{1c}$ concentration of about 4–30 ng/μL is needed for detection. Consequently, developing a high sensitivity, low cost, reliable, portable and user-friendly biosensor for $HbA_{1c}$ detection is necessary. Surface modification has been employed for numerous applications in various fields. The self-assembled monolayer (SAM) is a prevalent and effective biomolecule immobilization process for impedance measurement. The typical advantages of SAMs are that they are ultra-thin, well ordered and stable; however, the most important advantages include the enhancement of biocompatibility and replacement of nonspecific sites on the surface (Jiang et al., 2003). In this study, the thiophene-3-boronic acid (T3BA) is utilized to modify gold surfaces. The short chain structure of T3BA decreases the spatial distribution interference and the reaction influence between electrodes and $HbA_{1c}$.

An interdigitated ring-shaped array (IDRA) microelectrode (Liu et al., 2000) has been applied for miniaturizing the thin-layer radial flow cell to enhance the detection sensitivity. An IDRA microelectrode allows the cells to distribute uniformly on the surface of a working electrode by maintaining a thin diffusion layer between the electrode and analyte. An IDRA microelectrode has all the advantages of an interdigitated array (IDA) as well as microelectrodes such as the high Faraday current. IDA microelectrodes can be applied to electrochemical detectors for high-performance liquid chromatography (HPLC), selective detection of different biomolecules and microbore liquid chromatographic detection.

Various detection technologies based on different theories exist, including optics, electrochemistry, radioactivity and piezoelectric principles (Velasco and Mottram, 2003). In this study, impedance analysis is employed to detect the impedance between electrodes by providing a small sinusoidal voltage at a particular frequency range. When the voltage is applied to form a loop, an electric field arises, and the impedance can be calculated by Ohm's law. By utilizing different SAMs, impedance measurements can detect various targets, such as small-molecules (Hleli et al., 2006), cells (Mishra et al., 2005), DNA (Gooding, 2002) and proteins (Ferreira et al., 2010). Biomolecules immobilized by SAM can be detected by measuring the electrical signal through the electrode surface (Berggren et al., 2001).

## 2. Electrode design

The planar interdigitated ring electrode (PIRE) array utilizes positive dielectrophoresis (p-DEP) to solve the low uniformity problem in patterning cells of the microfluidic chip (Hsiung et al., 2008). Due to the interaction between DEP force and hydrodynamic force, a PIRE array can move and control cells in order to produce a uniform dielectrophoretic cell patterning (DCP), which in turn can promote the response and reproducibility of cell-based biosensors.

Consisting of a capture electrode and measurement electrode, the chip has the function of centralizing and detecting, which realizes the capture and measurement on the same electrode. By utilizing AC electro-osmosis (ACEO) and dielectrophoresis (DEP), effective concentrations and uniform distributions of quantum dots can be controlled (Sin et al., 2009). Due to this technique, $HbA_{1c}$ approaches the surface of the electrodes, which facilitates the binding reaction between $HbA_{1c}$ and electrodes.

### 2.1. Structure design

Compared with the parallel facing electrode (Chuang et al., 2012), the interdigital electrode is more convenient and easier to fabricate by microelectromechanical systems (MEMS). Moreover, the main advantage of the interdigital electrode is that the electric field is concentrated on the surface of electrode. In order to realize the centralization of $HbA_{1c}$, application of the ring structure is necessary (Sin et al., 2009). Therefore, the normal square-structured interdigital electrode is replaced by a ring structure, which improves the non-uniform electric field problem (Sun et al., 2007), efficiently decreases the electric field split and improves the detection stability.

The ring-shaped interdigital electrodes (RSIDEs) are integrated with active manipulation of quantum dots and the advantage of bi-spiral electrodes (Guo et al., 2005). Finally, this structure applied as the measurement electrode with the ability to concentrate $HbA_{1c}$ on the surface of the electrode and accomplish concentrated capture and detection on the same electrode is possible.

### 2.2. COMSOL simulation

COMSOL Multiphysics is an engineering, design, and finite element analysis software environment for the modeling and simulation of any physics-based system. In this study, COMSOL was utilized to simulate the electric field on the electrode surface. The buffer solution for $HbA_{1c}$ is phosphate buffered saline (PBS), which has a conductivity ($\sigma$) of 1.6 S/m and a relative permittivity ($\varepsilon_r$) of 80. The electrode material is gold (Au). Regularizing those parameters and exchanging the radius of rings can produce different electric field gradients. Employing different electric field gradients and different input voltages for the two electrodes creates several functions, such as concentrating and accumulating $HbA_{1c}$ in the center of the chip and on the electrode surface, respectively. There are two modes in this study, namely, the center-concentration mode and surface-accumulation mode.

Fig. S1(a) and (b) are the schematic diagrams of the center-concentration mode in the COMSOL simulation. When electrode P is 5 V, electrode N is 5 V, and the outermost external ring is the ground, this system can produce an electric field where the external ring is larger than the internal ring. The electric field of this system can form a concentrated force which drives $HbA_{1c}$ from the external ring to the internal ring and centralize.

Fig. S1(c) and (d) are the schematic diagrams of the surface-accumulation mode in the COMSOL simulation. When the electrode P is 5 V, electrode N is −5 V, and the outermost external ring is ground, this system can produce an electric field where the internal ring is larger than the external ring. The most critical factor of this system is that the electric field gradient decrease from the internal ring to the external ring, while the capture electrode electric field is less than all other electric field. The electric field of this system can form a downward force which drives $HbA_{1c}$ to approach the capture electrodes.

The center-concentration mode causes $HbA_{1c}$ to concentrate more effectively, which promotes more and more $HbA_{1c}$ to approach the measurement region. Thus, a larger amount of $HbA_{1c}$ can simultaneously participate in the binding reaction with T3BA (on the measurement electrode). The surface-accumulation mode causes $HbA_{1c}$ to distribute more uniformly, which facilitates the binding reaction between $HbA_{1c}$ and T3BA on the measurement electrode. Thus, more non-binding T3BA can interact with $HbA_{1c}$ in the same sample thereby increasing the coverage of $HbA_{1c}$ on the measurement electrode. Due to this, chip sensitivity can be increased and reaction time decreased.

## 3. Materials

Fig. 1(a) shows the completed RSIDEs. In the chip process, the substrate utilized a $75 \times 25$ mm microscopic glass slide for the deposition of gold, which has a superior biocompatibility.

The chromium (Cr) thickness, which serves as an adhesion layer, is 200 nm and was sputtered onto the glass slides. Following this, gold (Au), with a thickness is 800 nm, was sputtered onto the glass slides using an E-beam evaporator. Afterwards, the gold on the glass slides was formed into different patterns via standard photolithographic techniques, and then etched in accordance with Cr and Au etching solutions. Lastly, the glass slides were rinsed with acetone to strip off the photoresist.

T3BA, the empirical formula of which is $C_4H_5BO_2S$ (Sigma, St. Louis, MO, USA), was utilized to modify the surface of the electrode and form a SAM (Park et al., 2008). The $HbA_{1c}$ was obtained from Exocell Incorporated. Anti-hemoglobin, immunoglobulin (IgG) conjugated with fluorescein isothiocyanate (FITC) and phosphate buffer saline (PBS: pH 7.4, 0.2 g KCl, 1.44 g $NaHPO_4$, 8 g NaCl and 0.24 g $KH_2PO_4$ in 1:l deionized water) were purchased from Sigma–Aldrich Chemical Corporation.

## 4. Experimental methods

### 4.1. Electrode modification

T3BA was dissolved in a 10 mM ethanol solution and utilized to modify the electrode surface. Before the glass slide was immersed into the T3BA ethanol solution, it was exposed to UV cleaning for 20 min. Afterwards, the glass slide was rinsed with acetone, isopropanol and deionized water, and dried with nitrogen. The glass slide was immersed in the T3BA ethanol solution for 12 h at 27 °C with mild vibrations. Through a sulfur-gold bond, thiophene molecules binded to the gold electrode surface. The residual T3BA, adsorbed on the surface via non-covalent bonds, was cleaned with 95% degassed-ethanol in an ultrasonic cleaner for three times, and then dried with nitrogen. All experiments of this study were implemented in 24 h after electrode modification so as to maintain the best integrity of the SAM (Flynn et al., 2003).

### 4.2. Experimental condition examination

Certain experimental conditions, such as the driving signal and reaction time of $HbA_{1c}$, which influence the uniformity and quantity of the $HbA_{1c}$ coating, are important factors throughout the experiments. Other experimental conditions, such as the pH value of PBS and reaction temperature, have been completed in our previous study (Chuang et al., 2012). In the present study, all samples of $HbA_{1c}$ were dissolved in the PBS (pH value of 8.5) and reacted at room temperature, which was $26 \pm 1$ °C. This environment represents the best cis–diol interaction conditions between T3BA and $HbA_{1c}$ (Chuang et al., 2012). The other samples of anti-hemoglobin and IgG-FITC were diluted in normal PBS and reacted at the aforementioned room temperature.

#### 4.2.1. Driving signal of $HbA_{1c}$

Before impedance measurements of $HbA_{1c}$, the electrode should be given a driving signal to concentrate $HbA_{1c}$ on the surface of the electrode. In this study, two square waves, the frequencies and voltages of which were the same but the phases had a difference of 180°, were provided to each electrode. Afterwards, in order to determine the best driving frequency, frequencies of 500, 1000, 1500 and 2000 Hz were, respectively, provided

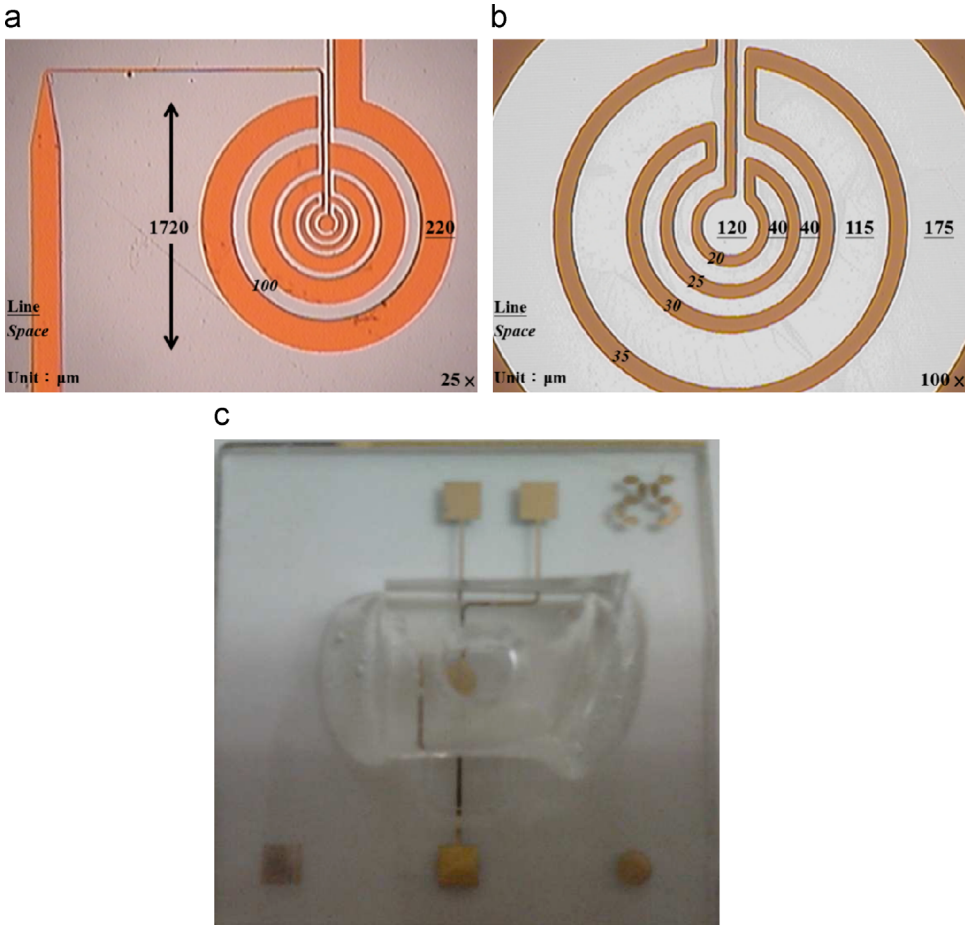


**Fig. 1.** (a) Microscopic image of completed ring-shaped interdigital electrodes and (b) impedance measurement chip fabricated with the PDMS chamber.

to the electrode. Lastly, the distribution uniformity of $HbA_{1c}$ was estimated via the fluorescence labeling method.

There are three steps of FITC anti-rabbit IgG immobilization on the electrode. First, 20 μL $HbA_{1c}$ sample, which had a concentration of 100 ng/μL, was dripped on the electrode that had been modified with T3BA, and provided the square wave driving signal for 30 min to centralize and immobilize $HbA_{1c}$. Afterward, the electrode was rinsed with PBS three times to clean the nonspecific adsorption of $HbA_{1c}$, and then dried with nitrogen. Second, the 20 μL anti-hemoglobin sample, with a concentration of 10 ng/μL, was dripped on the electrode that had been immobilized with $HbA_{1c}$, and reacted for 30 min. In the next step, the electrode was rinsed with PBS three times to clean the nonspecific adsorption of anti-hemoglobinthen, and then dried with nitrogen. Third, the 20 μL IgG-FITC sample, with a concentration of 1 mg/mL, was dripped on the electrode that had been immobilized with anti-hemoglobin and $HbA_{1c}$, and reacted for 30 min. After the reaction event, the electrode was rinsed with PBS three times to clean the nonspecific adsorption of IgG-FITC, and then dried with nitrogen.

Lastly, a Nikon ECLIPSE 80i fluorescence microscope and a CCD camera (Evoluting VF, Q-imaging, USA) were used to capture the fluorescent images. FITC was excited by a hydrargyrum lamp at a wavelength of 450–490 nm and the profile data intensity obtained from Image-Pro Plus 5.0 (Media Cybernetics, USA).

### 4.3. Impedance measurement

Fig. 1(b) shows the impedance measurement chip. At first, the T3BA-modified electrode was combined with the PDMS chamber to fabricate the impedance measurement chip. Precision Impedance Analyzers (Kayne Kerr Inc., 6440B) were connected to the platform which loaded the chip. Afterward, the impedance analyzer was utilized in accordance with short circuit and open circuit standard calibrations to self-calibrate before measurement. After calibration, and due to the capacitive characteristic of the device, the impedance phase angle should be −90° before the sample was dripped.

After setting up the experimental platform, five steps were needed to detect $HbA_{1c}$. First, 20 μL of PBS was dripped into the PDMS chamber and covered the electrode, then the impedance amplitude and phase angle were measured. Second, the 20 μL $HbA_{1c}$ sample was dripped into the PDMS chamber and covered the electrode, after which the chip was rinsed with deionized water and dried with nitrogen. Third, two electrodes were applied with two square waves to concentrate $HbA_{1c}$ close to the surface of the electrodes. Fourth, the electrodes were rinsed with deionized water and dried with nitrogen. And lastly, 20 μL of PBS was dripped into the PDMS chamber and covered the electrode, then the impedance amplitude and phase angle were measured as in first step. Protein detection is analyzed by the deviation of before–after impedance.

In this study, all impedance measurements applied an AC voltage of 100 mV by 6440B to record the impedance amplitude and phase angle from 0.5 to 20 kHz, as well as being implemented at a room temperature of 26 ± 1 °C and humidity of 40 ± 5%.

## 5. Results and discussion

### 5.1. Fluorescence labeling

The image and intensity of fluorescence is utilized to confirm whether $HbA_{1c}$ forms a stereo-structure binding on the gold electrodes. The distribution of $HbA_{1c}$ on the gold electrodes is observed via fluorescence labeling through anti-hemoglobin and IgG-FITC. The experiments' standard entails the most uniform distribution of $HbA_{1c}$ and best fluorescence intensity.

Fig. 2 is the image of fluorescence labeling after applying 1.5 kHz, 0.5 $V_{pp}$ and 0/180° square waves for the electrodes, and the intensity of fluorescence along the yellow line compared with various frequencies. These jagged lines demonstrate the flatness and intensity which represent the distribution condition of $HbA_{1c}$. At no function, the distribution of $HbA_{1c}$ is neither uniform nor immobilized at the center or edge of the electrodes, as shown in Fig. S2(a). At 0.5 and 1 kHz, the distribution of $HbA_{1c}$ is not uniform and mostly concentrated at the center of the electrodes, as shown in Fig. S2(b) and (c). At 1.5 kHz, the distribution of $HbA_{1c}$ is uniform and immobilized well, as shown in Fig. S2(d). At 2 kHz, the distribution of $HbA_{1c}$ is not uniform and concentrated mostly at the electrode edges, as shown in Fig. S2(e). At 1.5 kHz, the fluorescence intensity is the greatest while the standard deviation is the least, not only along the line but also in the areas.

From the results above, the optimal conditions utilized to centralize and immobilize $HbA_{1c}$ were a frequency of 1.5 kHz, a voltage of 0.5 $V_{pp}$ and a phase of two electrodes with a difference of 180°.

### 5.2. Detection of various concentrations of $HbA_{1c}$

In this study, in order to estimate the detectable range for clinical diagnosis application, various concentrations of $HbA_{1c}$, ranging from 1 to 100 ng/μL in 10 mM PBS (pH 8.5) were employed. The before–after impedance was analyzed from the measured data of magnitude (|Z|) and phase ($\theta$). Regardless of being before or after $HbA_{1c}$ successful immobilization on the electrodes, both utilized PBS as the background solution during measurement. Thus, the deviation of impedance was calculated as a percentage from:

$$\Delta|Z| = \frac{|Z|_{after} - |Z|_{before}}{|Z|_{before}} * 100\% \quad (1)$$

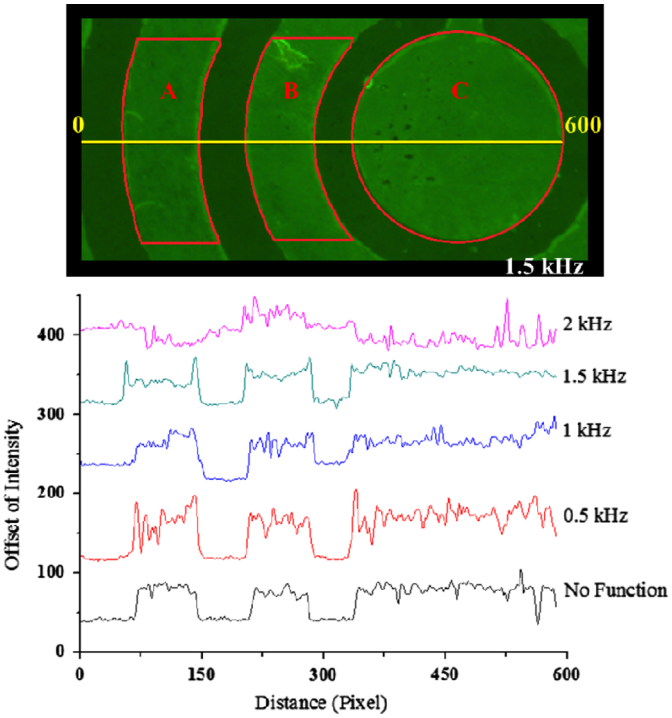


**Fig. 2.** Fluorescence labeling image after applying 1.5 kHz, 0.5 $V_{pp}$ and 0/180° square waves to the electrodes, and the intensity of fluorescence along the yellow line compared with no function, 0.5 kHz, 1 kHz, and 2 kHz. (For interpretation of the references to color in this figure caption, the reader is referred to the web version of this article.)

Fig. 3 is the before–after deviation of impedance at various concentrations of $HbA_{1c}$ and demonstrates that the least phase point (1.5 kHz) is much closer to the capacitance characteristic. It is possible that this could be due to the capacitive effect of the modified interface. The increasing percentages of impedance deviation are proportional to the logarithmic value of various concentrations in the range from 1 to 100 ng/μL.

### 5.3. Electric circuit model

In the electrical impedance measurement, the simplified equivalent electric circuit model was utilized to explain the behavior of the interface between electrodes and solution. The interface variations change the measurement results. When the material, such as T3BA and $HbA_{1c}$, is immobilized between the electrode and the solution, a dielectric layer with characteristics similar to the capacitance is formed. However, the surface of the electrode could not be entirely covered by T3BA or $HbA_{1c}$, thus there are numerous holes on the dielectric layer which render the electrode similar to the porous electrode. These holes formed the resistance characteristic, which is theoretically infinite for an ideal insulator or when no redox species are present, and are in parallel with the capacitance caused by the dielectric layer.

#### 5.3.1. Electric circuit model before $HbA_{1c}$ immobilization

Fig. 4(a) is the simplified equivalent electric circuit model of the RSIDEs before $HbA_{1c}$ immobilization. Assume the left electrode is symmetric to the right electrode so as to simplify the model for ease of analysis, where $C_s$ is the capacitance caused by PBS, $R_s$ is the resistance caused by PBS, $C_{SAM}$ is the sum of $C_{SAM1}$ and $C_{SAM2}$ which in turn are the capacitances caused by T3BA, $R_{SAM}$ is the sum of $R_{SAM1}$ and $R_{SAM2}$ which themselves are the resistances caused by T3BA and theoretically infinite, and $R_{Au}$ is the sum of $R_{Au1}$ and $R_{Au2}$ which constitute the parasitic resistances of the electrodes.

$Z(\theta)_{before}$ is the effective impedance before $HbA_{1c}$ immobilization and can be described as

$$Z(\theta)_{before} = \left[R_{Au} + \frac{R_{SAM}}{1+(\omega C_{SAM}R_{SAM})^2} + \frac{R_s}{1+(\omega C_s R_s)^2}\right] -j\left[\frac{\omega C_{SAM}{R_{SAM}}^2}{1+(\omega C_{SAM}R_{SAM})^2} + \frac{\omega C_s {R_s}^2}{1+(\omega C_s R_s)^2}\right] \quad (2)$$

where $\omega$ is the angular frequency.

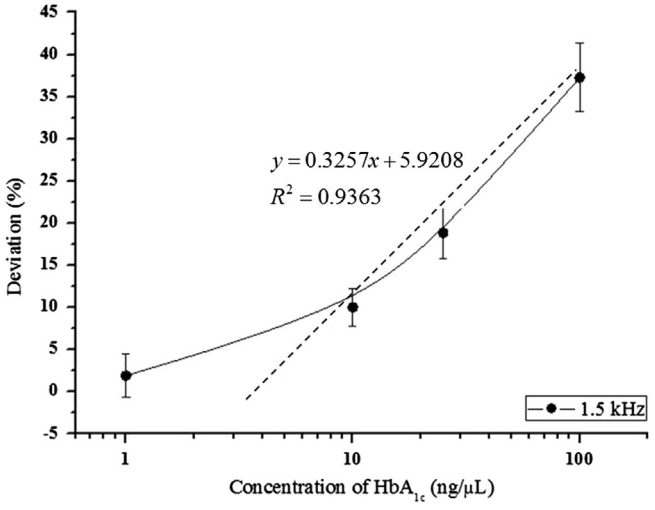


**Fig. 3.** Before–after deviation of impedance at various concentrations of $HbA_{1c}$ demonstrated at the least phase point, the frequency of which is 1.5 kHz.

#### 5.3.2. Electric circuit model after $HbA_{1c}$ immobilization

Fig. 4(b) is the simplified equivalent electric circuit model of the RSIDEs after $HbA_{1c}$ was immobilized, and assumes that the left and right electrodes are symmetric so as to simplify the model for ease of analysis, where $C_s$ is the capacitance caused by PBS, $R_s$ is the resistance caused by PBS, $C_{SAM}$ is the sum of $C_{SAM1}$ and $C_{SAM2}$ which are the capacitances caused by T3BA, $R_{SAM}$ is the sum of $R_{SAM1}$ and $R_{SAM2}$ which are the resistances caused by T3BA and theoretically infinite, $C_{HbA1c}$ is the sum of $C_{HbA1c1}$ and $C_{HbA1c2}$ which themselves are the capacitances caused by $HbA_{1c}$, $R_{HbA1c}$ is the sum of $R_{HbA1c1}$ and $R_{HbA1c2}$ which are the resistances caused by$HbA_{1c}$ and theoretically infinite, and $R_{Au}$ is the sum of $R_{Au1}$ and $R_{Au2}$ which are the parasitic resistances of the electrodes.

$Z(\theta)_{after}$ is the effective impedance after $HbA_{1c}$ was immobilized while $Z_{HbA1c}$ is the impedance caused by $HbA_{1c}$ immobilization, which is equal to $Z(\theta)_{after}$ minus $Z(\theta)_{before}$. After the calculation, the equation can be described as:

$$Z_{HbA1c} = \frac{R_{HbA1c}}{1+(\omega C_{HbA1c}R_{HbA1c})^2} - j\frac{\omega C_{HbA1c}{R_{HbA1c}}^2}{1+(\omega C_{HbA1c}R_{HbA1c})^2} \quad (3)$$

where $\omega$ is the angular frequency.

$\mathrm{Re}(Z_{HbA1c})$ and $\mathrm{Im}(Z_{HbA1c})$ are the real and imaginary parts of $Z_{HbA1c}$, respectively. The equation can be written as

$$\left\{\mathrm{Re}(Z_{HbA1c}) = ZCos(\theta)_{after} - ZCos(\theta)_{before} \quad (4)$$

$$\left\{\mathrm{Im}(Z_{HbA1c}) = ZSin(\theta)_{after} - ZSin(\theta)_{before} \quad (5)$$

According to Eqs. (3)–(5), and then substituting frequency, measured impedance and phase can obtain the simultaneous

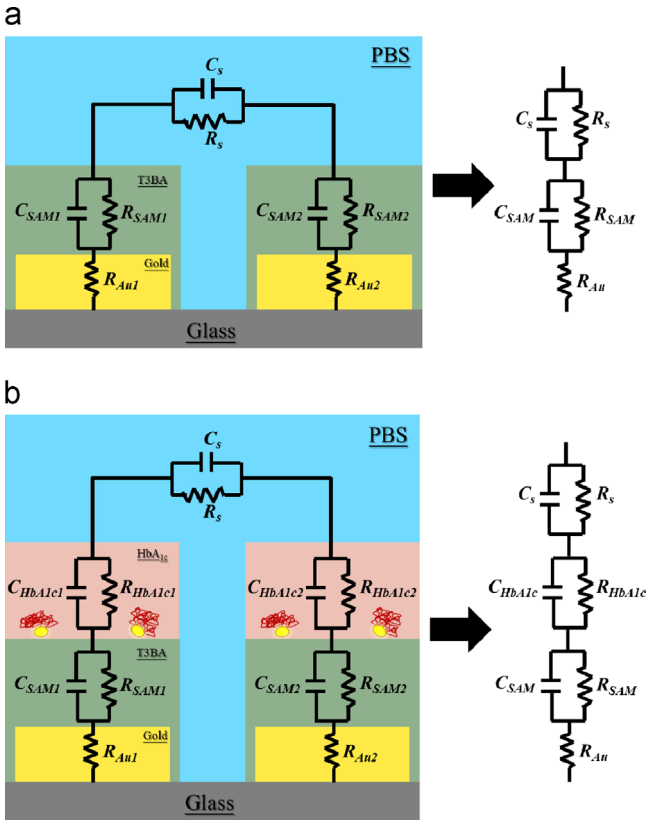


**Fig. 4.** Simplified equivalent electric circuit model of the ring-shaped interdigital electrodes (a) before $HbA_{1c}$ immobilization and (b) after $HbA_{1c}$ immobilization, where $C_s$ is the capacitance caused by PBS, $R_s$ is the resistance caused by PBS, $C_{SAM}$ is the sum of $C_{SAM1}$ and $C_{SAM2}$, $R_{SAM}$ is the sum of $R_{SAM1}$ and $R_{SAM2}$, $C_{HbA1c}$ is the sum of $C_{HbA1c1}$ and $C_{HbA1c2}$, $R_{HbA1c}$ is the sum of $R_{HbA1c1}$ and $R_{HbA1c2}$, and $R_{Au}$ is the sum of $R_{Au1}$ and $R_{Au2}$.

equation to solve the capacitance caused by $HbA_{1c}$ ($C_{HbA1c}$) in various concentrations of $HbA_{1c}$.

### 5.3.3. Electric circuit model analysis

Table 1 lists the parameters before and after $HbA_{1c}$ immobilization, which were obtained from the equivalent electric circuit model at various concentrations. $R_{Au}$ is approximate to 40 Ω, which was estimated by the area of the RSIDEs and the resistivity of gold. The resistance caused by PBS ($R_s$) and the capacitance caused by T3BA ($C_{SAM}$) have small variations between different measurements because of the process variation and respective chip fabrication. The capacitance caused by $HbA_{1c}$ ($C_{HbA1c}$) is the capacitive effect of the modified interface after $HbA_{1c}$ was immobilized where the electrode surface was covered by $HbA_{1c}$, the dielectric constant of which is approximately 11 (Chuang et al., 2012), which is less than PBS (80). Therefore, when the concentration increases, the covered area of the electrode surface and impedance caused by $HbA_{1c}$ increases, while the electron transfer ability and capacitance caused by $HbA_{1c}$ ($C_{HbA1c}$) decreases.

Figs. 5 and S3 are the compared measured impedance and phase in various concentrations of $HbA_{1c}$ with simulated impedance and phase, as obtained from the electric circuit model. As the result, the parameters obtained from the electric circuit model are matched to the result of the measurements in various concentrations of $HbA_{1c}$.

## 6. Conclusions

This study applied ring-shaped interdigital electrodes into $HbA_{1c}$ affinity biosensors on impedance measurement. The RSIDEs provided different functions for center-concentration and surface-accumulation to promote distribution uniformity and immobilization efficiency. The affinity method was utilized to recognize and immobilize $HbA_{1c}$ on T3BA-modified electrodes through the cis–diol reaction between $HbA_{1c}$ and boronic acid.

Results revealed that $HbA_{1c}$ was uniformly distributed and well-immobilized after two electrodes were provided square waves, frequency of which was 1.5 kHz, the voltage was 0.5 $V_{pp}$, and the phase difference was 180°, for 30 minutes. Afterwards, the $HbA_{1c}$ concentration from 1 to 100 ng/μL could be measured via the impedance analyzer at a frequency between 0.5 and 20 kHz and quantified based on the capacitive changes arisen from the surface of the RSIDEs.

The $HbA_{1c}$ affinity biosensor with the RSIDEs successfully detected various concentrations of $HbA_{1c}$. In addition, this device has the potential of point-care diagnostics due to its cheap, label-free and easy MEMS fabrication.

**Table 1**
Parameters obtained from the model in various concentrations of $HbA_{1c}$.

| Concentrations (ng/μL) | | 1 | 10 | 25 | 100 |
|---|---|---|---|---|---|
| Before $HbA_{1c}$ immobilized | $R_s$ (Ω) | 470.3 | 316.6 | 409.4 | 357.8 |
| | $C_{SAM}$ (nF) | 6.8 | 8.8 | 6.2 | 6.7 |
| After $HbA_{1c}$ immobilized | $R_s$ (Ω) | 470.3 | 316.6 | 409.4 | 357.8 |
| | $C_{SAM}$ (nF) | 6.8 | 8.8 | 6.2 | 6.7 |
| | $C_{HbA1c}$ (nF) | 97.8 | 73 | 30.5 | 16.3 |

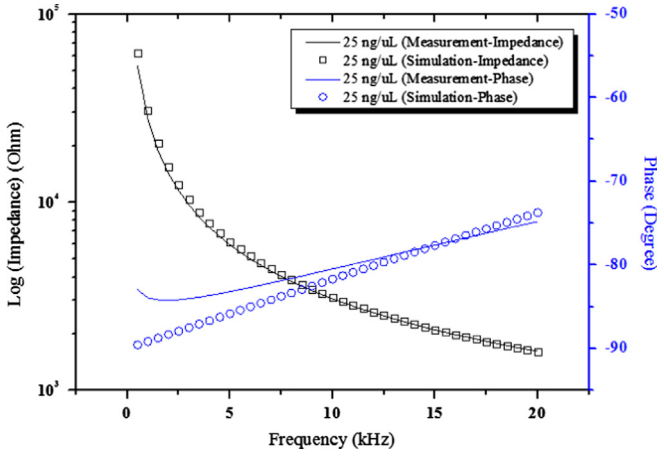


**Fig. 5.** Impedance and phase after immobilization of 25 ng/μL $HbA_{1c}$, where the black and blue solid lines are the measured impedance and phase, respectively, while the square and circle dots are simulated impedance and phase, respectively. (For interpretation of the references to color in this figure caption, the reader is referred to the web version of this article.)

## Appendix A. Supporting information

Supplementary data associated with this article can be found in the online version at http://dx.doi.org/10.1016/j.bios.2013.05.059.

## References


Amos, A.F., McCarty, D.J., Zimmet, P., 1997. Diabetic Medicine 14 (5), S1–S85.
Berggren, C., Bjarnason, B., Johansson, G., 2001. Electroanalysis 13 (3), 173–180.
Bunn, H.F., Haney, D.N., Gabbay, K.H., Gallop, P.M., 1975. Biochemical and Biophysical Research Communications 67 (1), 103–109.
Busto, M.E.C., Montes-Bayón, M., Añónb, E., Senz-Medel, A., 2008. Journal of Analytical Atomic Spectrometry 23 (5), 758–764.
Chuang, Y.C., Lan, K.C., Hsieh, K.M., Jang, L.S., Chen, M.K., 2012. Sensors and Actuators B: Chemical 171-172, 1222–1230.
Fanga, L., Li, W., Zhou, Y., Liu, C.C., 2009. Sensors and Actuators B: Chemical 137 (1), 235–238.
Ferreira, A.A.P., Alves, M.J.M., Barrozo, S., Yamanaka, H., Benedetti, A.V., 2010. Journal of Electroanalytical Chemistry 643 (1-2), 1–8.
Flynn, N.T., Tran, T.N.T., Cima, M.J., Langer, R., 2003. Langmuir 19 (26), 10909–10915.
Gooding, J.J., 2002. Electroanalysis 14 (17), 1149–1156.
Guo, X.S., Chen, Y.Q., Pan, M., Wang, L.R., 2005. Journal of Zhejiang University—Engineering Science 39 (7), 957–961.
Halámeka, J., Wollenbergera, U., Stöckleina, W.F.M., Warsinkea, A., Schellera, F.W., 2007. Analytical Letters 40 (7), 1434–1444.
Hleli, S., Martelet, C., Abdelghani, A., Burais, N., Jaffrezic-Renault, N., 2006. Sensors and Actuators B: Chemical 113 (2), 711–717.
Hsiung, L.C., Yang, C.H., Chiu, C.L., Chen, C.L., Wang, Y., Lee, H., Cheng, J.Y., Ho, M.C., Wo, A.M., 2008. Biosensors and Bioelectronics 24 (4), 869–875.
Huang, C.J., Chien, H.C., Chou, T.C., Lee, G.B., 2011. Microfluidics and Nanofluidics 10 (1), 37–45.
Jenkins, M., Ratnaike, S., 2005. Clinical Chemistry and Laboratory Medicine 41 (6), 747–754.
Jiang, X.C., Beyer, T.P., Li, Z., Liu, J., Quan, W., Schmidt, R.J., Zhang, Y., Bensch, W.R., Eacho, P.I., Cao, G., 2003. Journal of Biological Chemistry 278 (49), 49072–49078.
King, H., Rewers, M., 1993. WHO Ad-Hoc diabetes reporting group. Diabetes Care 16 (1), 157–177.
Krishnamurti, U., Steffes, M.W., 2001. Clin. Chem. 47 (7), 1157–1165.
Lasseter, T.L., Cai, W., Hamers, R.J., 2004. Analyst 129 (1), 3–8.
Li, Y.C., Pfüller, U., Larsson, E.L., Jungvid, H., Galaev, I.Yu., Mattiasson, B., 2001. Journal of Chromatography A 925 (1-2), 115–121.
Liu, Z., Niwa, O., Kurita, R., Horiuchi, T., 2000. Journal of Chromatography A 891 (1), 149–156.
Mishra, N.N., Retterer, S., Zieziulewicz, T.J., Isaacson, M., Szarowski, D., Mousseau, D.E., Lawrence, D.A., Turner, J.N., 2005. Biosensors and Bioelectronics 21 (5), 696–704.
Park, J.Y., Chang, B.Y., Nam, H., Park, S.M., 2008. Analytical Chemistry 80 (21), 8035–8044.
Přibyl, J., Skládal, P., 2005. Analytica Chimica Acta 530 (1), 75–84.
Přibyl, J., Skládal, P., 2006. Biosensors and Bioelectronics 21 (10), 1952–1959.
Qu, L., Xia, S., Bian, C., Sun, J., Han, J., 2009. Biosensors and Bioelectronics 24 (12), 3419–3424.
Sin, M.L.Y., Gau, V., Liao, J.C., Haake, D.A., Wong, P.K., 2009. Journal of Physical Chemistry C113 (16), 6561–6565.
Son, S.Y., Han, Y.D., Lee, K.H., Yoon, H.C., 2010. Bulletin of the Korean Chemical Society 31 (7), 2103–2106.
Stöllner, D., Stöcklein, W., Scheller, F., Warsinke, A., 2002. Analytica Chimica Acta 470 (2), 111–119.
Sun, T., Green, N.G., Gawad, S., Morgan, H., 2007. IET Nanobiotechnology 1 (5), 69–79.

Tanakaa, T., Izawaa, K., Okochia, M., Limb, T.K., Watanabeb, S., Haradab, M., Matsunagaa, T., 2009. Analytica Chimica Acta 638 (1), 186–190.
Velasco, M.N., Mottram, T., 2003. Biosystems Engineering 84 (1), 1–12.
Xue, Q., Bian, C., Tong, J., Sun, J., Zhang, H., Xia, S., 2011a. Biosensors and Bioelectronics 26 (5), 2689–2693.
Xue, Q., Bian, C., Tong, J., Sun, J., Zhang, H., Xia, S., 2011b. Sensors and Actuators A: Physics 169 (2), 282–287.
Xue, Q., Bian, C., Zhang, H., Xia, S., 2010. Proceedings of the IEEE on Mechatronics & Embedded Systems & Applications, 208–212.